Zero-dimensional turbulence modeling of a spark ignition engine in a Miller cycle " Dethrottling " approach using a variable valve timing system

Marcellin Perceau, Philippe Guibert, Stéphane Guilain

▶ **To cite this version:**

Marcellin Perceau, Philippe Guibert, Stéphane Guilain. Zero-dimensional turbulence modeling of a spark ignition engine in a Miller cycle " Dethrottling " approach using a variable valve timing system. Applied Thermal Engineering, 2021, 199, pp.117535. 10.1016/j.applthermaleng.2021.117535 . hal-03405668

HAL Id: hal-03405668

https://hal.sorbonne-universite.fr/hal-03405668

Submitted on 27 Oct 2021

HAL is a multi-disciplinary open access archive for the deposit and dissemination of scientific research documents, whether they are published or not. The documents may come from teaching and research institutions in France or abroad, or from public or private research centers.

L'archive ouverte pluridisciplinaire **HAL**, est destinée au dépôt et à la diffusion de documents scientifiques de niveau recherche, publiés ou non, émanant des établissements d'enseignement et de recherche français ou étrangers, des laboratoires publics ou privés.

ZERO-DIMENSIONAL TURBULENCE MODELING OF A SPARK IGNITION ENGINE IN A MILLER CYCLE « DETHROTTLING » APPROACH USING A VARIABLE VALVE TIMING SYSTEM

Marcellin PERCEAU[1,2,*], Philippe GUIBERT[2], Stéphane GUILAIN[1]

[1]Renault – Guyancourt, France

[2]Sorbonne Université, Institut Jean le Rond d'Alembert, France
2 Place de la gare de Ceinture, 78210 Saint Cyr l'Ecole

[*]Corresponding author: marcellin.perceau@renault.com; marcellin.perceau@sorbonne-universite.fr
Final draft: Applied Thermal Engineering
DOI: 10.1016/j.applthermaleng.2021.117535

Highlights :

- A complete 0D model with in-cylinder aerodynamic prediction and turbulent combustion is proposed
- Analytical calculation of quantities reduces the cost and time of the predictions
- The effect of a VVT system on the performance of an EIVC Miller cycle engine is investigated
- Reduction in pumping losses results in benefits of up to 1% over a wide range of engine loads

Abstract:

The Miller cycle, using an early inlet valve closing, can significantly improve the overall efficiency of a spark ignition engine during partial load operations. The shorter valve intake event minimizes the need for throttling the air and so reduces the pumping losses. This method is known as "dethrottling". Indeed, the use of a variable valve lift system makes it possible to combine two different cam profiles in an engine, one for the full load operations and one for the partial loads. The benefits of this strategy, combined with a variable valve timing (VVT) system, will be explored using a new 0D model. This model can take into account the strong changes of in-cylinder turbulence generated by the VVT and their effects on the combustion. Efforts have been made to reduce the model's reliance on external inputs. Therefore, analytical calculations of quantities, such as the flame radius, have been favored. The Miller cycle can lead to indicated efficiencies around 44% and the addition of a VVT system can improve the overall efficiency up to 1% over a wide range of engine loads.

Keywords : Miller Cycle, Dethrottling, VVT, 0D model, Turbulence, Flame radius

1 THE MILLER CYCLE

1.1 Context

While the transportation sector was the origin of 15% of the CO2 released into the atmosphere in 1990, its proportion reached 18% in 2016 [1]. This increase combined with global warming has prompted the European Parliament to restrict gas emissions through the Euro 6 standard. Despite the emergence of electric vehicles, the internal combustion engine still has a future. In 2035, in a scenario of high environmental regulations, 77.2% of vehicles sold worldwide will be gasoline engines, only 11.9% will be fully electric and 0.1% will be fuel cell powered [2]. The sector is therefore evolving and many innovations are being introduced to improve internal combustion engines.

Vehicles will tend to be electrified [3], [4] by switching to a 48V system, that will for example allow the use of e-turbo [5], [6], or by a more complete hybridization. New components that will allow engines to operate optimally over a wider range of operating conditions will be introduced [7]. We can mention variable compression ratio with, for example, a modification of the classic connecting rod and crank system. The system can be almost completely modified, as is the case with the MCE-5 engine [8], the crank section can also be redesigned, as the Infinity VC-turbo engine [9], and the connecting rod can vary its stroke while being integrated into the engine without major modifications [10]–[12]. Conventional turbocharger are likely to be equipped with a variable turbine section [13], [14]. The timing and lift of the valves can be modified by different systems during engine operation [15]–[18]. The number of cylinders in operation may also vary according to the required load [19]–[22]. Fluid properties can be altered to achieve better performance by injecting water and working on EGR systems [23]–[25]. For example, water, injected during compression, cools the mixture by evaporation, which limits knocking and allows the use of higher compression ratios. The work done to reduce mechanical friction is revealed in most articles featuring new engines. Engineers are also experimenting new combustions by testing new fuels [26]–[30] and new types of ignition, such as Mazda's HCCI Skyactiv engine, which ignites the air-gasoline mixture at a high compression ratio [31]–[34], and a microwave ignition system that replaces traditional spark plugs [35], [36]. Energy recovery by combined cycle is also studied [37]–[39], for example the heat extracted downstream of the catalytic converter can be used in a Rankine cycle where the turbine will drive the crankshaft [40].

The application of over expanded cycles such as the Atkinson and Miller cycles allows high efficiencies to be achieved, can be coupled with the above solutions [28], [41]–[46] and generally requires only minor engine modifications. Changes will be made mainly to the intake valve timing.

1.2 Presentation of the cycle

The Miller cycle is part of the over-expanded cycle family. Its expansion stroke is longer than its compression one.

James Atkinson, a British engineer, was the first to work on over expanded cycle. He wrote three patents on engines working with complex connecting rods. The first one was written in 1886 and describes an opposed piston engine in which the volume at the end of the intake stroke is lower than the volume at the end of the expansion [47]. The second one is a four stroke engine presented in 1887 [48]. It's Atkinson's most famous engine and the most frequently presented one when talking about Atkinson cycle. The volume at the end of the expansion stroke is twice time larger than the one at the end of the compression stroke. According to the author, this leads to an engine that is more economical than any other gas-engine built before. Atkinson wrote a patent, in 1892, about an over-expanded cycle engine closer to the classical four stroke internal combustion engine. However, few engines were produced so information about it can't be easily found. For more details about this engine the reader can refer to Marshall's paper on the history of Atkinson's machines [49]. An over-expanded cycle engine with such a complex connecting rods system is not actually used in a vehicle. Yet, research has been made on the subject, we can mention BMW [50] and Honda with the EXlink engine [51], [52]. The major disadvantages are friction losses, inertia of the extra parts and the bigger space needed. The interest for this kind of system seems to grow when they allow variable compression ratio like, for example, MCE-5 engine [7] and Nissan's VC-turbo [9]. We can also add that Honda is working on its EXlink engine and tends to variable compression [54].

Another way to unlink the compression and the expansion stroke is to act on the time when the inlet valves are closing. When closing the valves before or after the bottom dead center the intake stroke is shorter than the expansion one. For an early inlet valve closing (EIVC), before the BDC, we have $V_{IVC} < V_{BDC}$ and so a smaller effective compression ratio. For a late inlet valve closing (LIVC), after the BDC, part of the fluid inside the cylinder is pushed back into the intake manifold. This leads to the same situation as before with a fluid volume smaller than what the cylinder could have contained. This method has been for the first time used by the American engineer Ralph Miller. He invented a way to move forward or delay the intake valves closing progressively with the increase of the engine load, the main objective being to avoid knocking. He worked on a compression ignited engine, a spark ignited one and a two-stroke engine in three patents

respectively deposited in 1954 [55], 1956 [56] and 1957 [57]. The name Miller cycle is most of the time linked to an early inlet valve closing (EIVC) whereas the name Atkinson cycle is related to late inlet valve closing (LIVC). We'll use this convention for this paper.

1.3 Application Strategy

Recent years have seen the arrival of a new concept in the world of internal combustion engines: "downsizing". The aim is to reduce the size of engines by reducing the volume of the cylinders or, for example, by using three cylinders instead of four. These engines are also equipped with a turbocharger, allowing them to deliver the same power as a larger-displacement engine. This reduction in size reduces mass and friction, and thus reduces consumption. Manufacturers' interest in the Miller cycle seems to have stopped this trend. Indeed, the term "rightsizing" is starting to appear in automotive journals. Manufacturers use a "downsized" engine from their line of products and design a larger displacement engine, the increase in size coming from the extended expansion of the Miller cycle. Examples include Opel's Ecotec engines [58], [59], Volkswagen's TSI engines [60], Audi's TFSI [61] and also BMW's boxer engine for motorcycles [62]. The increase in displacement is mainly achieved by increasing the piston stroke. The low dead volume of the combustion chamber is therefore maintained, which allows to keep the compression ratio at the maximum before knocking and thus does not degrade the engine's efficiency.

The benefit obtained by running a Miller cycle on an engine whose expansion has been extended compared to a reference engine following an Otto cycle, with the same compression ratio, is a gain in mechanical work. Assuming that the combustion is the same for both engines, using the same amount of fuel, the gain in mechanical work implies a better thermal efficiency for the Miller engine. The benefits at full load of the rightsizing strategy have been studied in a previous study and can lead to a 3% improvement of the overall engine efficiency [63].

Another advantage of the Miller cycle is that it can reduce pumping losses that are the pressure losses introduced by the throttle valve when working at part load and during the intake stroke. This approach is called "dethrottling". The idea is not new and dates back to the 1980s [64], but advances in variable lift and valve timing systems have democratized its use [62], [65], [66]. The engine can have two camshafts, one for the high loads and one for the low loads. Shorter total lift duration can be used at part loads, the throttle use as a way to reduce the amount of air is then reduced. Therefore, the engine can follow an Otto, Atkinson or a Miller cycle at high loads and a Miller cycle at low loads. This strategy can then be adopted for many engine configurations.

1.4 Miller cycle limitations

One major issue with the Miller cycle is the losses of in-cylinder turbulence generated. Because of the shorter intake event, the Miller cycle leads to internal aerodynamic losses. The tumble movement is less intense, which leads to lower levels of turbulent kinetic energy at the top dead center. Yet it's well known that turbulence, by wrinkling the flame front, accelerates combustion and improves its stability. Aerodynamic deterioration has therefore a strong impact on engine efficiency and is an important factor to consider for the Miller cycle study.

The next parts of this paper present a method to compute the efficiency taking into account this change in internal aerodynamics and its effect on combustion.

It will then be applied to Miller cycle engine, with a short lift duration, and the benefits obtained by the installation of a variable valve timing (VVT) system on this engine will be calculated.

2 CYCLE MODELING

2.1 Governing physics

In this paper, a 0D model, developed with MATLAB, is used to compute the overall efficiency of a Miller cycle gasoline engine. Zero-dimensional models are a time and cost effective way to predict a combustion engine comportment [67]–[69]. These models are based on the conservation laws of mass and energy in which the system is discretized in homogeneous volumes.

During non-combustion phases, which are the intake, compression, expansion and exhaust phases, the model considers one homogeneous volume. The

fluid, being a mixture of burned and un-burned gases, has the same properties in the whole cylinder. Quantities depend on the crank angle, which is an image of the time for a known speed rotation, so we'll use the term 0D model. Mass, temperature and pressure are computed according to the ideal gas law and the conservation of mass and energy [70].

$$V\frac{dP}{dt} + P\frac{dV}{dt} = rT\frac{dm}{dt} + mr\frac{dT}{dt} \quad (1)$$

$$\frac{dm}{dt} = \frac{dm_{in}}{dt} + \frac{dm_{out}}{dt} + \frac{dm_{in}^{bfl}}{dt} + \frac{dm_{out}^{bfl}}{dt} \quad (2)$$

$$\frac{d(m.u)}{dt} = -P\frac{dV}{dt} + \frac{dQ_{wall}}{dt} + h_{in}\frac{dm_{in}}{dt} + h_{cyl}\left(\frac{dm_{out}}{dt} + \frac{dm_{in}^{bfl}}{dt}\right) + h_{out}\frac{dm_{out}^{bfl}}{dt} \quad (3)$$

Leakage flows such as blowby and injection mass gains are not taken into account.

During the combustion phase, the model considers two homogeneous volumes, one central volume containing the burned gases, which are the exhaust products, and the other one containing the fresh gas composed of fuel, air and residual gases. The pressure is supposed to be the same in both sides. Quantities will be calculated using the same laws as for the non-combustion phases and will be applied in both regions. The conservation of energy is written as follow :

$$\frac{d(m_u u_u)}{dt} = -P\frac{dV_u}{dt} + \frac{dQ_{wall}^{u}}{dt} + h_u\frac{dm_u}{dt} \quad (4)$$

$$\frac{d(m_b u_b)}{dt} = -P\frac{dV_b}{dt} + \frac{dQ_{wall}^{b}}{dt} - h_u\frac{dm_u}{dt} \quad (5)$$

In parallel, in-cylinder turbulence is estimated during the whole cycle by a turbulence model (2.2). The level of turbulence reached at the end of the compression phase then allows a combustion sub-model (0) to calculate the variations in burnt mass. All quantities are described at the end of this paper.

The cylinder volume can be calculated, for each crank angle, according to geometrical parameters. The connecting rod length here is about 138 mm. Flows through valves depend on upstream and downstream conditions. The mass flow rates differ from the ideal values by introducing a discharge coefficient that depends on the valve lift. These flows can also be choked if the upstream and downstream conditions are critical [71]. Moreover, the flow is considered as an ideal compressible fluid with thermodynamic properties changing according to the composition and the temperature. The fuel is considered to be isooctane and the calculations are performed at stoichiometric conditions. Exchanges Q_{wall} at the cylinder head, piston, valves and cylinder liner are simulated. The model uses the Woschni formula to determine the transfer coefficients, common values were used for the constants [72], [73].

2.2 Prediction of the in-cylinder turbulence

Prediction of the in-cylinder turbulence during the cycle is made by a $K-k-\varepsilon$ model. It provides an estimation of the turbulent velocity at the end of compression by calculating the mean kinetic energy (MKE) of the flow, the turbulent kinetic energy (TKE), the turbulent dissipation (ε) and the kinetic moment of the large-scale aerodynamic motion (tumble).

This model is a combination of $K-k$ [74] and $k-\varepsilon$ [75] models and its first presentation occurred in 2017 [76]. Several models of this type exist today. They differ mainly on the way to describe the energy flow into the cylinder, on the production of turbulence from the non-tumble mean flow and on the creation of turbulence by the tumble movement decay. For this model, the choice was made to adopt the general structure of the equations of the first Fogla model [76] with an in-cylinder mass flow multiplied by the coefficient C_T and to integrate the tumble decay function resulting from an analytical calculation of Kim's model [77]. This choice avoids additional heavy CFD calculations. Moreover, reduced equations, for the production of turbulence from the non-tumbling flow, will be used in the way of Bozza [78].

Fig. 1 shows the evolution of in-cylinder energy and its decomposition to produce turbulence during the intake and the compression stroke. The intake flow is divided into two using the tumble coefficient C_T, which is an image of the torque generated by the tumble movement [79]. It then participates either in the generation of the tumble movement or a non-tumble flow. Then, using the constant C_a, the non-

tumble flow contributes either to the creation of mean kinetic energy (MKE) or directly to the generation of turbulence (TKE). The turbulence at the end of the compression phase then results from the collapse of the tumble movement and by the phenomenon of cascade from large to small scales.

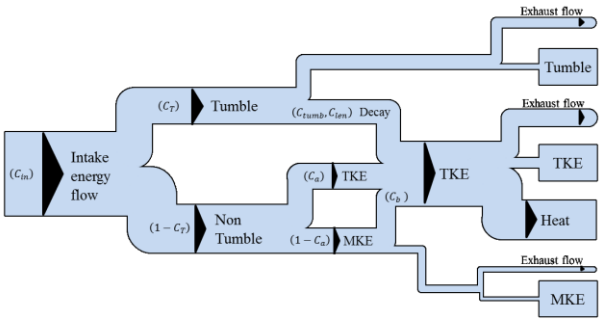

Fig. 1 : In-cylinder energy evolution

The model is composed of four equations that describe the evolution of the MKE where $K = \frac{1}{2}U^2$ (U mean flow velocity), the TKE where $k = \frac{3}{4}u'^2$ (u' turbulent velocity), the dissipation rate ε and the tumble angular momentum L :

$$\frac{dmK}{dt} = (1 - C_a)\dot{E}_{in} - \dot{m}_{out}K + mK\frac{\dot{\rho}}{\rho} - P_K \quad (6)$$

$$\frac{dmk}{dt} = C_a\dot{E}_{in} - \dot{m}_{out}k + P_k - m\varepsilon + C_{tumb}m\dot{k}_\psi \quad (7)$$

$$\frac{dm\varepsilon}{dt} = \dot{E}_{in}\frac{\sqrt{k}}{L_g} - \dot{m}_{out}\varepsilon + P_\varepsilon - \left[C_{\varepsilon 2} + \frac{C_\mu\eta^3\left(1-\frac{\eta}{\eta_0}\right)}{1+\beta\eta^3}\right]\frac{m\varepsilon^2}{k} + C_{tumb}m\dot{k}_\psi\frac{\sqrt{k}}{L_g} \quad (8)$$

$$\frac{dL}{dt} = \dot{L}_{in} - L\frac{\dot{m}_{out}}{m} - \dot{L}_\psi \quad (9)$$

The first three equations of the model contain the kinetic energy creation term $\dot{E}_{in}$ which depends on the constant C_{in} representing a loss of kinetic energy at the cylinder intake. The creation term of the angular momentum for the tumble flow $\dot{L}_{in}$ is calculated with the tumble radius $r_t = \sqrt{I_z/m}$ resulting from the calculation of the inertia momentum I_z. The two incoming energy terms write as follows:

$$\dot{E}_{in} = (1 - C_T)\frac{\dot{m}_{in}}{2}C_{in}v_{in}^2 \quad (10)$$

$$\dot{L}_{in} = C_T\dot{m}_{in}\sqrt{C_{in}}v_{in}r_t \quad (11)$$

Where v_{in} is the in-cylinder isentropic velocity, $\dot{m}_{in}$ the in-cylinder mass flow and C_T the tumble coefficient. The tumble radius r_t can be calculated for a pentroof and a simplified pancake cylinder head geometry with the method described by Kim [77] and the pentroof angle is referred as $\beta \approx 17°$. The formula is presented in the Appendix A. Fig. 2 presents the evolution of r_t compared with CFD results from a paper by Bozza [78]. The CFD result is also presented with an offset to mask differences due to engine diameters. In this paper, the firing top dead center (fTDC) is at 360°CA. The curves have similar shapes but differ slightly for crank angles close to the fTDC, probably because of the different cylinder head geometry and pentroof angles.

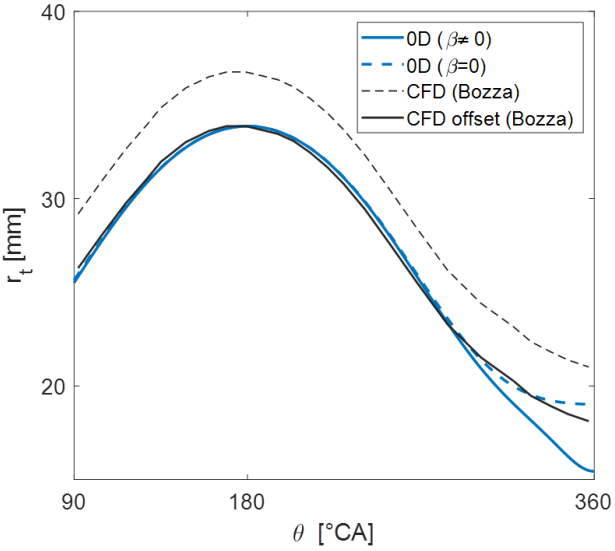

Fig. 2 : Tumble radius evolution

The term $\dot{k}_\psi$ represents the turbulent energy brought by the loss of angular momentum $\dot{L}_\psi$ of the tumble movement. They are linked by the following relation:

$$\dot{L_\psi} = \frac{I_z}{L}m\dot{k_\psi} \quad (12)$$

Where $\dot{k_\psi}$ can be calculated analytically, see Appendix A. A tumble decay function f_d can be used to compare calculations to previous works, it writes as follow [76], [80]:

$$f_d = \frac{I_z}{L^2}\frac{r_t}{\sqrt{k}}m\dot{k_\psi} \quad (13)$$

Fig. 4 shows its value, according to the instantaneous stroke to bore evolution, as well as that of decay

functions derived from CFD calculations by Fogla [76] and Kim [80]. The x-axis is shifted to erase the effect of the geometry and thus observe the effect of this function when the three engines are at TDC for the same x value. The closer the piston gets to the TDC, the more the rotational energy of the tumble is transformed into small-scale turbulence. We can see that the function is between the two CFD curves when the piston approaches the TDC. The analytical calculation of f_d is therefore a good way to reduce calculation times.

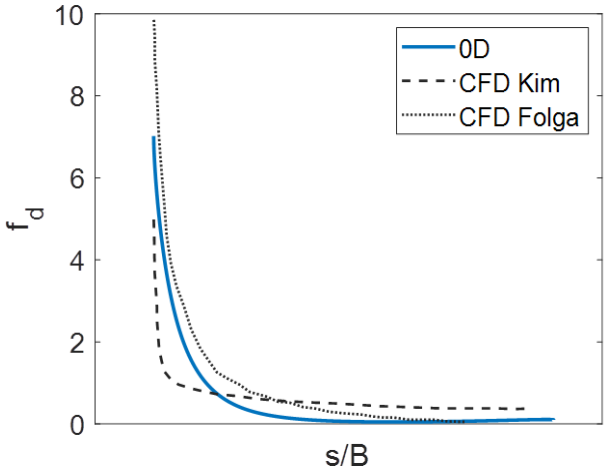

Fig. 4 : Tumble decay function evolution

This system includes two production terms P_k and P_ε which model the production of TKE, and the associated dissipation. The production is carried out by a cascade phenomenon from large scale structures to smaller ones, represented by P_K, and by compression effects :

$$P_k = P_K + \frac{2}{3}mk\frac{\dot{\rho}}{\rho} - \frac{2}{3}mv_t\left(\frac{\dot{\rho}}{\rho}\right)^2 \quad (14)$$

$$P_\varepsilon = \frac{\varepsilon}{k}\left[C_{\varepsilon 1}P_K + \left(\frac{2}{3}C_{\varepsilon 1} - C_{\varepsilon 4}\right)mk\frac{\dot{\rho}}{\rho} - \frac{2}{3}C_{\varepsilon 1}mv_t\left(\frac{\dot{\rho}}{\rho}\right)^2\right] \quad (15)$$

$$P_K = 2C_b mv_t\frac{2K}{L_g^2} \quad (16)$$

Where $L_g = C_{len}\min(stroke, bore)$ is a characteristic length and $v_t = C_\mu k^2/\varepsilon$ is the turbulent viscosity. The constant values, presented in the symbols part, were selected from Ref. [81]. These production terms come from the reduction of 3D equations in the Bozza manner [78] and the derivation is made in the appendix of the referenced paper [63].

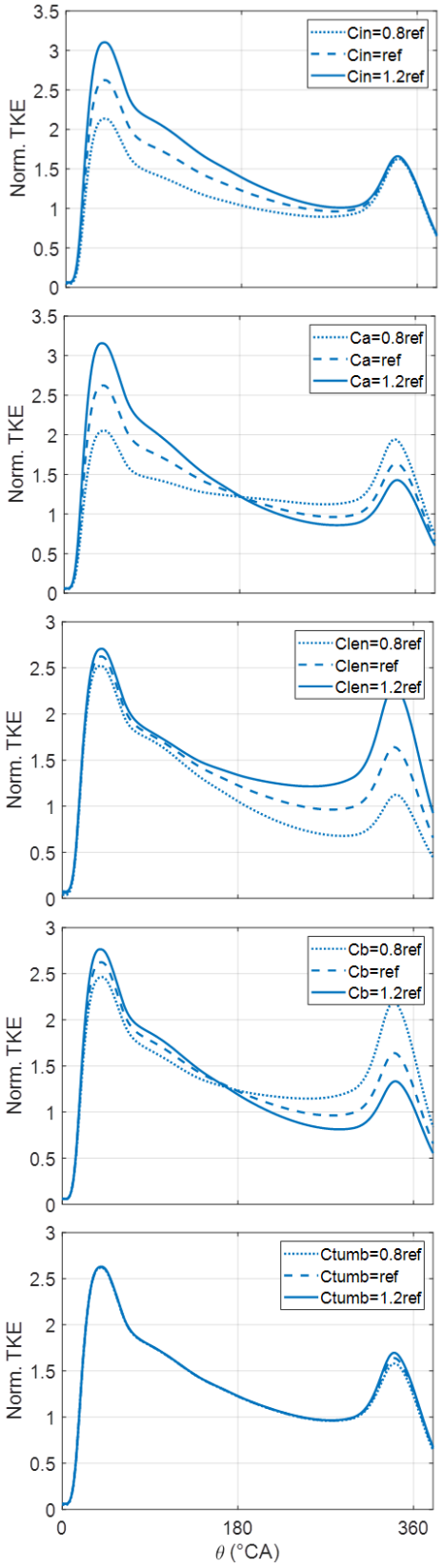

Fig. 3 : Effect of a 20% variation in the tuning constants

This model includes five tuning constants $C_a, C_{in}, C_b, C_{len}$ and C_{tumb}. Fig. 4 shows the effect of a 20% change in the value of the constants on the turbulent kinetic energy curve normalized by $0{,}5u_p^2$ where $u_p = 2N.s/60$ is the mean speed of the piston, according to the stroke s and the rotational speed N. The model is tuned on the results of 3D-CFD calculations performed with the CONVERGE software. It generates the meshing automatically and uses an orthogonal base grid set to 4mm. Adaptive Mesh Refinement allows maximizing the accuracy while keeping a reasonable computing time in complex areas. The boundary conditions were measured on a single-cylinder test engine performing complete engine cycles and bench-measured flow parameters are imposed on the intake valves. The RANS turbulent model RNG (Renormalization Group) $k-\epsilon$ is used. The rotation speed is 2000rpm and the calculation are made wide open throttle. The five tuning constants were identified (2.2) to overlap the 0D and 3D results on the VTT offset=0°CA line. In the manner of De Bellis [82], by making the tuning constants C_{len} and C_{tumb} depend on the IVC angle θ_{IVC}, the turbulent velocity can be estimated for different VVT offset. Constant values are presented in Table 1.

Table 1 : Turbulent constant values

Constant	Value
C_a	$0{,}3$
C_{in}	$0{,}05$
C_b	$5{,}7$
C_{len}	$0{,}0044\ \theta_{IVC} - 0,098$
C_{tumb}	$0{,}05\ \theta_{IVC} - 0,4$

Comparison between 0D and CFD results are made at motoring conditions without combustion. As we can see in Fig. 5, 0D and 3D results are close for angles greater than 300°CA for the four compared VVT offset. Therefore, in-cylinder turbulence is well estimated for the angular range corresponding to the combustion phase.

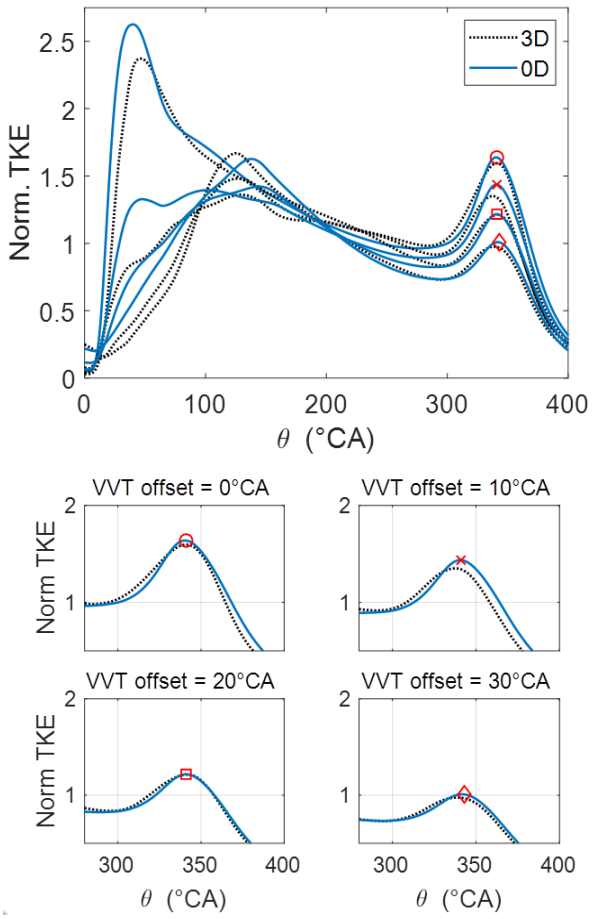

Fig. 5 : CFD comparison – 2000rpm

Fig. 6 shows the effect of a variation in the rotation speed. The TKE is still normalized by $0{,}5u_p^2$ and u_p is calculated at 2000rpm for each curve, so the augmentation in TKE can be seen.

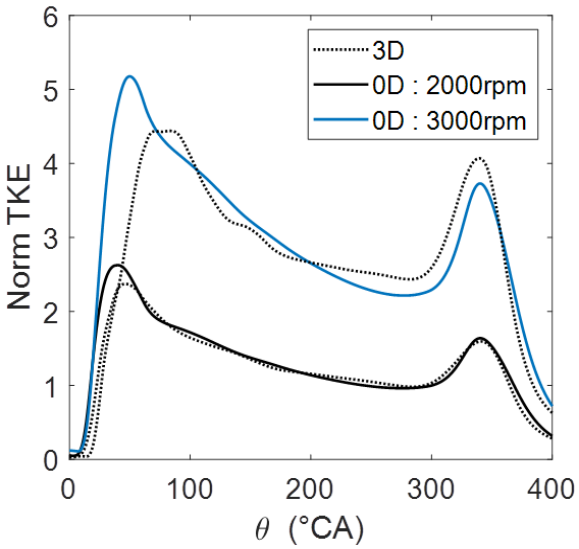

Fig. 6 : Effect on a variation in the rotational speed – VVT offset=0°CA

From comparison with CFD results, we can say that the turbulent model can predict in-cylinder turbulence at the end of the compression stroke. It uses one set of tuning constants to predict a VVT offset and an augmentation in the rotational speed.

2.3 Turbulent combustion modeling

In a gasoline engine, turbulence wrinkles the flame front and changes its propagation speed. For this model, the combustion chamber is separated into two zones, with an entrained gas zone and a fresh gas zone. The entrained gas zone has an intermediate zone, consisting of fresh and burnt gases, which models the flame front and in which the fresh gases are transformed into burnt gases, Fig. 7.

Combustion is modeled in two stages. First, a certain amount of fresh gas enters the entrained zone [83], [84]:

$$\frac{dm_e}{dt} = \rho_u A_f S_T \tag{17}$$

Where ρ_u is the unburned gases density, A_f the unwrinkled flame area and S_T the turbulent speed.

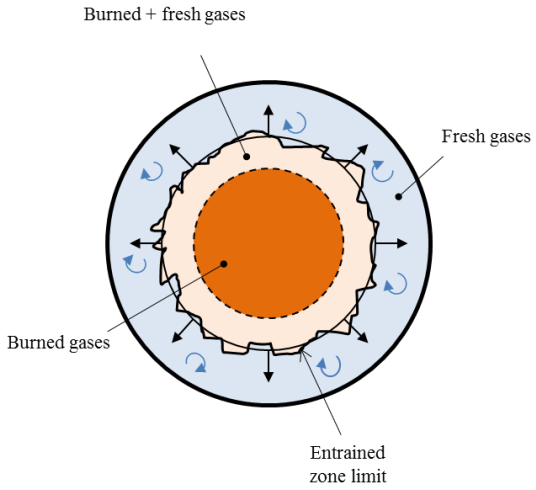

Fig. 7 : Turbulent combustion modeling

The turbulent speed S_T can be derived from the following relation [84]:

$$S_T = S_L + C_s u' \left(1 - \frac{1}{1 + C_k \frac{r_f^2}{l_t^2}} \right) \tag{18}$$

Where r_f is the unwrinkled flame radius, u' the turbulence intensity, l_t the turbulent length scale and C_s and C_k two constants. The laminar flame speed S_L depends on the unburned gas temperature, the in-cylinder pressure and is calculated with typical gasoline values [71], [72], [85].

The unwrinkled flame area A_f and the flame radius r_f can be derived from analytical calculations according to the burned gas mass, Appendix B. Fig. 8 presents the normalized flame radius r_f/r_{cyl} evolution as a function of the fraction of burned mass (MFB). Black lines are calculated using the previous formulas and the blue area comes from GT Power calculations made for several combustion durations on three different engines, more details can be found in the reference paper [77]. Analytical calculations have been made for six engines with different geometries and for eight combustion durations from 25 to 60°CA (6×8 lines). Wiebe's law is used to generate the evolution of the burned volume V_b for different combustion durations and geometries, typical parameters for gasoline combustion are chosen ($a = 5$, $m = 2$) [71]. The

presented calculations provide a good estimation of the flame radius evolution.

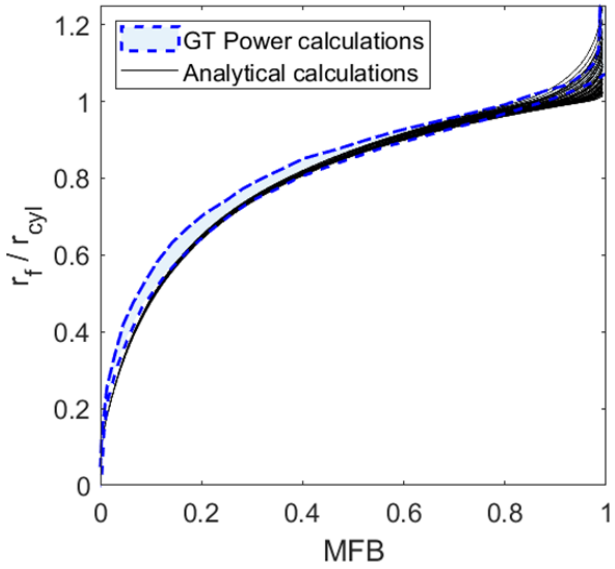

Fig. 8 : Normalized flame radius evolution

The second step of the modeling is to transform the fresh gas mass of the entrained zone, $m_e - m_b$, into burned gas. This transformation takes place in a characteristic time τ_{comb} and the increase in the mass of burnt gas is expressed by the relation [83], [84]:

$$\frac{dm_b}{dt} = \frac{m_e - m_b}{\tau_{comb}} \tag{19}$$

The characteristic time writes as follow :

$$\tau_{comb} = C_\lambda \frac{\lambda}{S_L} \;\; ; \;\; \lambda = \frac{\mu_u}{\rho_u u'} \tag{20}$$

Where C_λ is a constant and μ_u is calculated using a Sutherland law [86].

This model contains three constants that have been calibrated for a geometry engine close to the one studied in this paper by Mirzaeian [84]. We choose to keep the same values $C_k = 0{,}51$, $C_s = 1{,}37$ and $C_\lambda = 1{,}43$. Combustion stops when 99% of the fresh gas mass has been transformed into burned gas and, in the next part of this paper, combustion duration is defined as the time between ignition and the end of combustion.

3 APPLICATION TO A MILLER CYCLE VVT ENGINE

3.1 VVT load control

The power of a gasoline engine is generally regulated by an intake throttle valve. This operation disturbs the flow and the pumping work increases, which reduces the overall efficiency of the engine. One solution to limit intake restriction is to act on the valve timing. The quantity of air admitted by the engine will thus depend on the opening and closing times of the intake valves. Part of the engine load control will therefore be transferred to a VVT (Variable Valve Timing) system. The chosen system allows the law of the inlet cams to be shifted by 50°CA maximum. The objective of this study is to quantify the gains brought by this system when it replaces part of the use of the throttle valve for engine load control. The reference engine chosen follows a Miller cycle with an IVC of about 160°CA at 0,7mm lift (VVT offset : 0°CA) and has a 12,3 compression ratio. It is in a long stroke configuration with a bore to stroke ratio of about 0,85.

The VVT system allows an angular displacement of the intake valves lift law. The quantity of air admitted into the cylinder therefore varies with this offset and makes it possible, in part, to regulate the load. Indeed, the load represents the average pressure applied by the fluid on the engine piston during a cycle. It is therefore also strongly dependent on the combustion conditions of the air/fuel mixture. Fast combustion, starting at the right time at the end of the compression phase of the piston will result in a high load, a high pressure on the piston. Similarly, slow combustion starting too early or too late will create a low pressure on the piston, the engine will then have a low load.

The shift in the intake lift law changes the conditions under which fluid enters the cylinder, so the internal aerodynamic is affected by the VVT offset. Knowing that the level of turbulence at the end of compression modifies the duration of combustion, it is important to take this effect into account in this analysis. Fig. 9 presents the flowchart of the complete cycle modeling.

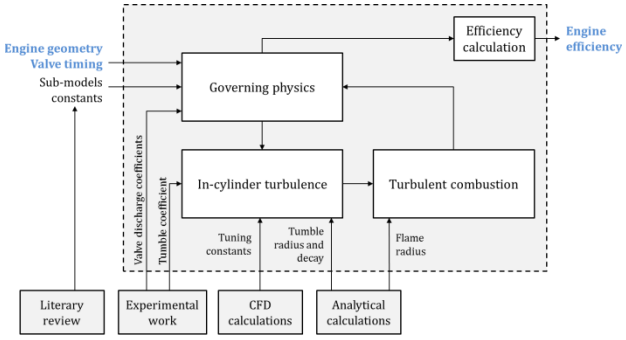

Fig. 9 : Complete model flowchart

Fig. 10 shows how the VVT impacts the level of turbulence and the evolution of the burned gas mass during combustion. The turbulence intensity u' is normalized by the piston speed u_p. Calculations were performed at wide open throttle, 2000rpm and combustion begins at 348°CA. The shift of the intake law is done in the direction of valve overlap, it creates an early intake valve closing. This advance of closing comes to degrade the level of turbulence at the end of compression, which can be seen in the central window of Fig. 10. As the turbulence level is reduced, the combustion time increases as we can see in the lower window. Indeed, we can notice that the curve corresponding to the maximum offset (VVT offset=50°CA) reaches its asymptote about 11°CA later than the curve corresponding to the minimum offset (VVT offset=0°CA). Moreover, we can notice that the final burned mass gas is less important when the offset is high, which shows that the early intake valve closing event has reduced the mass of air admitted by the engine.

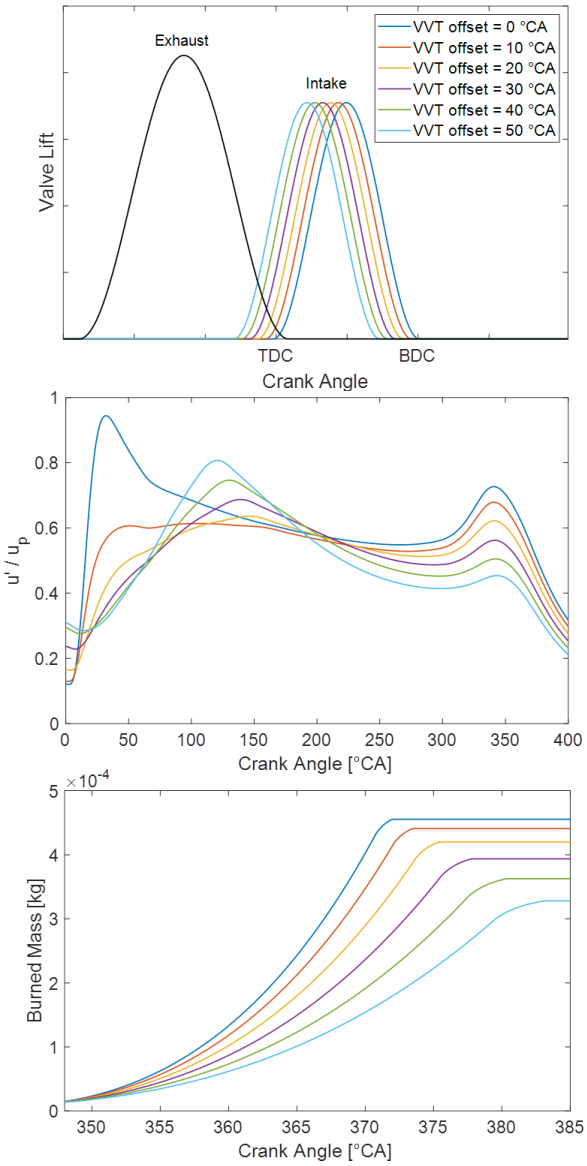

Fig. 10 : Effect of a VVT offset on the in-cylinder turbulence and on a burned gas mass

Slower combustion and a reduction in the mass admitted by the engine are in the direction of a reduction of the engine load. It is therefore the cumulative effect of the increase in combustion duration and the reduction in the mass admitted by the engine that allows the VVT system to reduce the load and replace the throttle.

Fig. 11 shows the engine load, IMEP (Indicated Mean Effective Pressure), as a function of the VVT offset. Calculations are made wide open throttle, at 2000rpm with ignition at 348°CA. The load can thus be regulated over a range of approximately 4bar without having to use the throttle valve.

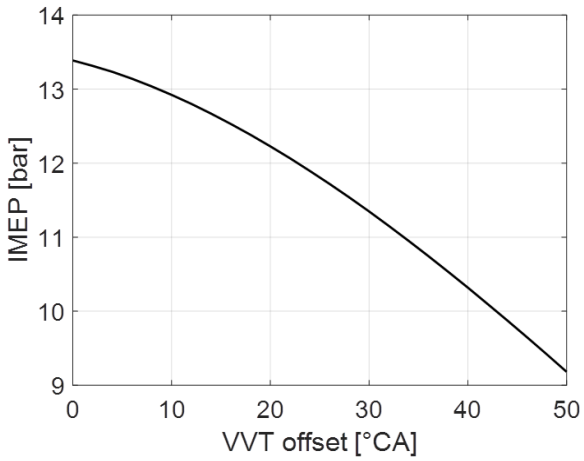

Fig. 11 : Engine load regulated by the VVT offset

3.2 Efficiency of the throttle Miller engine

In the next sections, a throttle engine and a VVT engine will be compared. The VVT engine has the same characteristics as the throttle engine but is equipped with a VVT system. Their efficiency will be estimated for every load and at 2000 and 3000rpm. This section focuses on the throttle engine.

The effect of the throttle is seen here as a pressure drop at the engine air intake. Let's introduce the coefficient "*throttle*" which represents a percentage of the ambient pressure. This coefficient is an approximation of the throttle valve opening and its variations allow the load to be adjusted. The intake pressure causes negligible changes in turbulence at the end of the compression stroke [80]. Therefore, changes in combustion characteristics, such as the combustion duration and the optimum ignition time, will mainly be due to the difference of in-cylinder mass generated by a throttle variation.

Before computing the efficiency, the optimal ignition angle must be found. Fig. 12 shows the engine indicated efficiency as a function of the ignition time at 2000rpm. We can see that the optimal ignition time (red markers) is between 348 and 349°CA. A more precise search for this optimum is then performed numerically by a software function using parabolic interpolation and the golden-section search method. This function is adapted to this case because the efficiency presents a unique maximum when it varies according to the ignition time. This research is carried out for any load at 2000 and 3000rpm. The mean optimal angle is 349,02°CA at 2000rpm and 347,59°CA at 3000rpm.

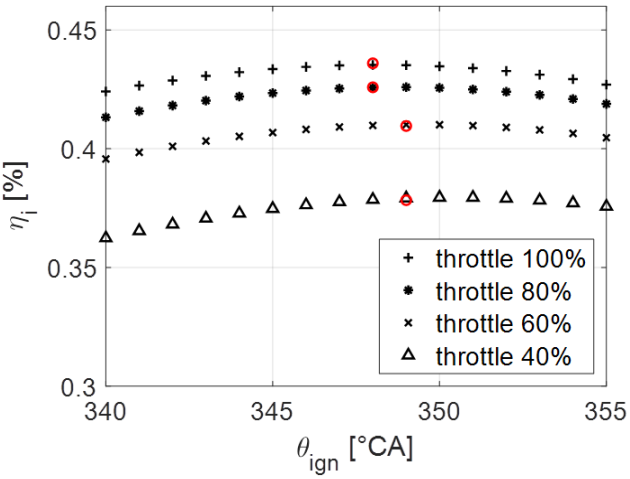

Fig. 12 : Indicated efficiency as a function of the ignition time for different loads – 2000rpm

Fig. 13 upper window shows the indicated efficiency of the throttle engine for all loads and optimum angles for both rotational speeds. The lower window presents the *throttle* coefficient as a function of the generated load. We can notice that the efficiency of the engine at 3000rpm is higher than at 2000rpm. This is an expected result. Indeed, the indicated efficiency is plotted, it does not include friction losses and the heat losses are lower when the rotation speed is high. We can also see that the Miller cycle is very efficient at full load, with an indicated efficiency around 44%.

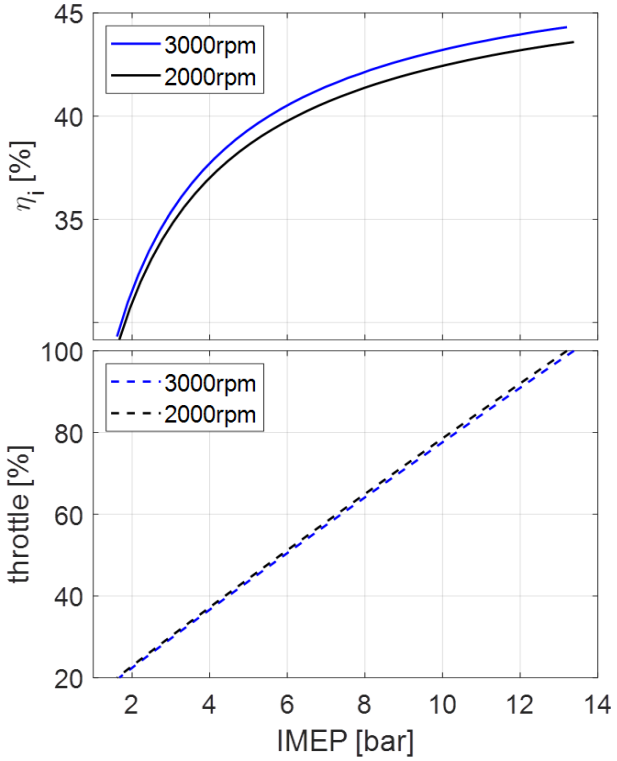

Fig. 13 : Throttle engine efficiency for all loads – 2000/3000rpm

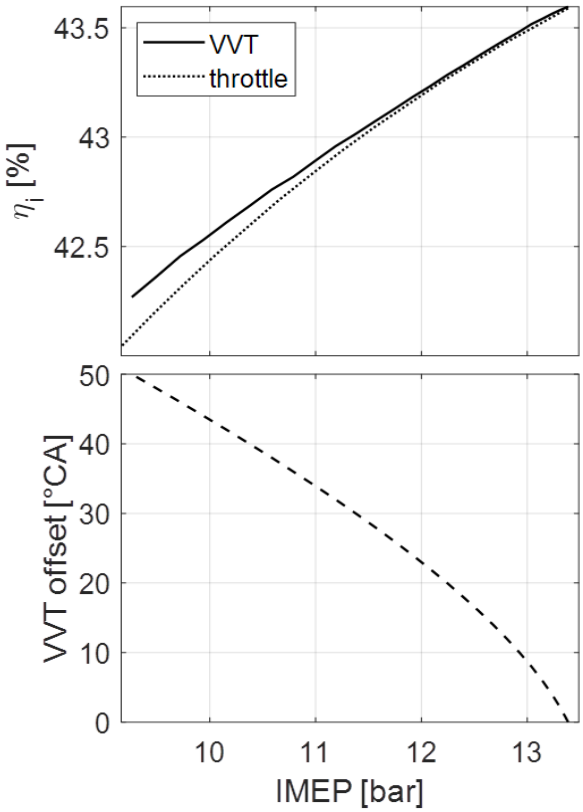

Fig. 14 : VVT and throttle efficiency – 2000rpm

3.3 Benefits of the VVT system

This section focuses on the VVT engine and the benefits this system can deliver on the throttle engine.

Fig. 14 shows the efficiencies of the throttle engine and of the same engine on which a VVT was installed, keeping the intake throttle fully open. We can see that the VVT improves the engine efficiency and allows load regulation, without throttle, over a range of 4,13 bar. In the same way as for the throttle engine, the optimal ignition time to achieve the best efficiency has been calculated. As we have seen in 3.1, the VVT can regulate the load partially by playing on the combustion time. Variations in combustion duration are not minor, so this optimization step is essential.

Table 2 shows the 50 percent burn angle (CA50) value according to the VVT offset value. For 2000rpm the mean value is 364,19°CA with a deviation of 0,37°CA and for 3000rpm it is 363,61°CA with a 0,47°CA deviation. The CA50 position is almost the same for every VVT offset value because the ignition angle has been computed for the best efficiency. It can also be seen that, because of higher turbulence intensity in Fig. 6, the combustion durations at 3000rpm are shorter than ones at 2000rpm.

Table 2 : Optimal ignition time and combustion duration for several VVT offset

N = 2000 rpm

VVT offset [°CA]	CA50 [°CA]	Combustion duration [ms]	[°CA]
0	364,32	2,00	24,06
10	364,40	2,11	25,29
20	363,99	2,22	26,68
30	364,03	2,37	28,44
40	364,52	2,54	30,49
50	363,63	2,67	32,10

N = 3000 rpm

VVT offset [°CA]	CA50 [°CA]	Combustion duration [ms]	[°CA]
0	363,10	1,41	25,36
10	363,31	1,49	26,91
20	363,30	1,60	28,75
30	363,76	1,73	31,08
40	363,96	1,86	33,56
50	363,08	1,99	35,76

Fig. 15 presents the advantages of using a VVT on an engine for all loads and at 2000 and 3000rpm. The VVT is firstly used to control the high loads at wide open throttle. When it reaches its limit, the throttle takes over to control the load. Benefits of using the VVT increase with the VVT offset. Afterwards, they almost remain stagnant for loads between 4 and 8 bar when throttle takes over, to then decrease to the minimum load. The efficiency benefits reach 1% over between 4 and 8 bar at 3000rpm and around 0,7% at 2000rpm. Therefore they apply to a large part of the engine's operating points. The cumulative total of all these gains is therefore not negligible during the real operation of the engine.

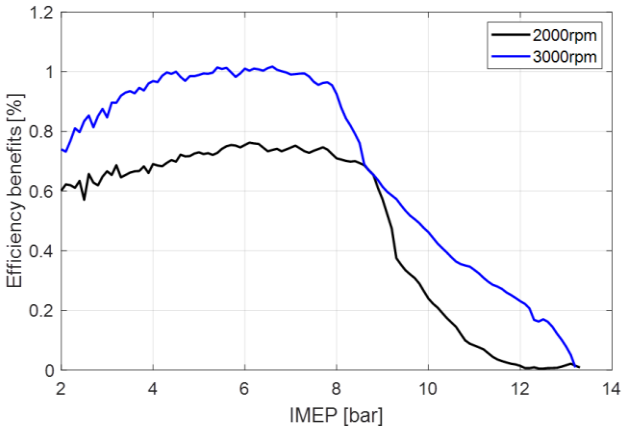

Fig. 15 : Efficiency benefits of using a VVT on an engine for all loads – 2000 and 3000rpm

CONCLUSION

A complete 0D model has been presented. It can predict in-cylinder turbulence and its effect on the combustion to provide an estimation of a SI engine efficiency. Moreover, efforts have been made to reduce the model's reliance on external inputs and thus reduce the cost and time of calculations. Analytical calculations of quantities such as the flame radius have been favored. This model can be used to study parameters causing variations in the aerodynamic such as a change in the lift law. It can provide an estimation of the overall efficiency and more specifically the benefits obtained by choosing one parameter value over another.

An application has been made on a Miller cycle engine. In the chosen configuration, the Miller cycle can provide a very good indicated efficiency of about 44% at full load. The benefits of using a VVT on this engine can go up to 1% over a wide range of loads. The sum of all these gains is not negligible during the real operation of the engine and leads to fuel consumption economies.

The study was conducted without taking into account acoustic effects. In a less throttled cycle, acoustic can improve the cylinder air filling and so achieve better efficiency. Therefore, the VVT benefits exposed may be minimized. The maximum offset was here fixed at 50°CA but systems with a wider range will generate more savings.

More data are needed to study the benefits of a wider range VVT. These data are necessary to verify that the turbulence generated by, for example, a

100°CA VVT offset is well predicted by the turbulent model. In the same way benefits from a variation in the lift (VVL) can be studied.

ACKNOWLEDGEMENTS

This work was supported by Renault SA, Guyancourt, France.

APPENDIX A

The tumble radius r_t and the tumble kinetic energy production $\dot{k_\psi}$ derivations were made using Kim's method [77]. Fig. 16 presents the simplified geometry of the combustion chamber.

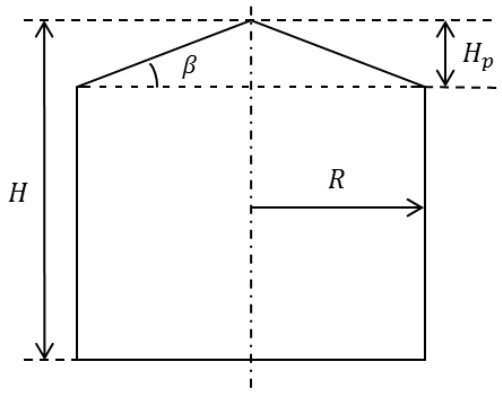

Fig. 16 : Combustion chamber simplified geometry

The tumble radius can be computed according to the following formula :

$$r_t = \left(\frac{1}{360V}.\left((64a^3 + 192a)R^5 + (45\pi a^2 + 90\pi)HR^4 + 120aH^2R^3 + 30\pi H^3R^2\right)\right)^{1/2} \quad (21)$$

Where $a = -\tan(\beta)$ and V is the instantaneous combustion chamber volume calculated with the classical formula [71].

The tumble kinetic energy production is computed using F_{a1} and F_{a2} formulas. It writes as follow :

$$\dot{k_\psi} = \nu_t \frac{L^2}{\rho^2 V} F_{a2}^2 F_{a1} \quad (22)$$

$$F_{a1} = \pi R^2 H\left(\frac{H^2}{4R^4} - \frac{7}{6R^2} + \frac{5}{2H^2}\right) + \left(\frac{(128a^2 + 1152)aR^3}{315H^2} + \frac{\pi a^2 R^2}{3H} - \frac{16aR}{15} + \frac{aH^2}{3R}\right) \quad (23)$$

$$F_{a2} = \frac{840H}{R^2}.(256a^3R^3 + 175\pi a^2 HR^2 + 672aH^2R + 210\pi H^3)^{-1} \quad (24)$$

The instantaneous stroke H is needed to compute r_t and $\dot{k_\psi}$. It is not directly derived from V, it depends on the pentroof volume V_p.

$$H = \frac{V - V_p}{\pi R^2} + H_p \quad (25)$$

$$V_p = 4\int_{x=0}^{R}\int_{y=0}^{H_p + ax}\int_{z=0}^{\sqrt{R^2 - x^2}} dxdydz = \pi R^2 H_p + \frac{4R^3 a}{3} \quad (26)$$

APPENDIX B

This appendix presents the flame radius analytical calculations. We assume a centered spherical propagation. At the beginning of the combustion, the burnt gas volume is semi-spherical and not constrained by the walls. It can then come into contact with the piston or the liner. At the end of combustion, the exhaust gas volume is in contact with the piston and the liner.

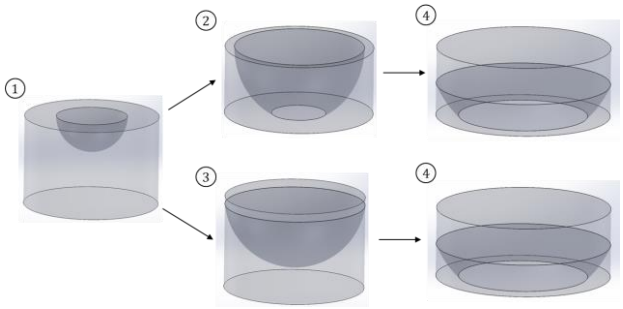

Fig. 17 : Unwrinkled flame area propagation

The flame radius $r_{f,i}$ is first calculated knowing $V_{b,i}$ for the i case, Fig. 17, which then allows to calculate $A_{f,i}$:

$$V_{b,1} = \frac{2}{3}\pi r_{f,1}^3 \qquad A_{f,1} = 2\pi r_{f,1}^2 \tag{27}$$

$$V_{b,2} = \frac{\pi\left(r_{f,2}^2 - h^2\right)h}{3} + \frac{2}{3}\pi r_{f,2}^2 h \qquad A_{f,2} = 2\pi r_{f,2} h \tag{28}$$

$$V_{b,3} = \frac{2}{3}\pi r_{cyl}^2 h_f + \frac{2}{3}\pi r_{f,3}^3\left(1 - \frac{h_f}{r_{f,3}}\right) \qquad A_{f,3} = 2\pi r_{f,3}^2\left(1 - \frac{h_f}{r_{f,3}}\right) \tag{29}$$

$$V_{b,4} = \frac{2}{3}\pi r_{cyl}^2 h_f + \frac{\pi\left(r_{f,4}^2 - h^2\right)h}{3} + \frac{2}{3}\pi r_{f,4}^2\left(h - h_f\right) \qquad A_{f,4} = 2\pi r_{f,4}\left(h - h_f\right) \tag{30}$$

Where h is the combustion chamber height derived from the stroke, r_{cyl} the cylinder radius and $h_f = \sqrt{r_f^2 - r_{cyl}^2}$.

ACRONYMS

BDC	Bottom Dead Center
TDC	Top Dead Center
fTDC	firing Top Dead Center
CA	Crank Angle
EIVC	Early Inlet Valve Closing
LIVC	Late Inlet Valve Closing
IVC	Inlet Valve Closing
IMEP	Indicated Mean Effective Pressure
MKE	Mean Kinetic Energy
TKE	Turbulent Kinetic Energy
MFB	Mass Fraction Burned
SI	Spark Ignition
VVT	Variable Valve Timing
VVL	Variable Valve Lift

SYMBOLS

P	In-cylinder pressure	Pa
V	In-cylinder volume	m^3
T	In-cylinder temperature	K
m	In-cylinder mass	kg
θ	Crank angle	$°CA$
r	Mass-specific gas constant	$J.kg^{-1}.K^{-1}$
$\dot{m}_{in}$	In-cylinder mass flow	$kg.s^{-1}$
$\dot{m}_{out}$	Out-cylinder mass flow	$kg.s^{-1}$
bfl	Backflow	$-$
u	Specific internal energy	$J.kg^{-1}$
h	Specific enthalpy	$J.kg^{-1}$
K	MKE	$m^2.s^{-2}$
k	TKE	$m^2.s^{-2}$
ε	Dissipation rate	$m^2.s^{-3}$
L	Angular momentum	$kg.m^2.s^{-1}$
ρ	Density	$kg.m^{-3}$
$\dot{E}_{in}$	In-cylinder energy	$kg.m^2.s^{-3}$
$\dot{L}_{in}$	In-cylinder angular momentum	$kg.m^2.s^{-3}$
P_K	MKE production	$kg.m^2.s^{-3}$
P_k	TKE production	$kg.m^2.s^{-3}$
P_ε	Dissipation rate production	$kg.m^2.s^{-4}$
$\dot{k}_\psi$	Tumble kinetic energy production	$m^2.s^{-3}$
$\dot{L}_\psi$	Tumble angular momentum loss	$kg.m^2.s^{-2}$
f_d	Tumble decay function	$-$
v_{in}	Isentropic in-cylinder velocity	$m.s^{-1}$
L_g	Characteristic length	m
r_t	Tumble radius	m
I_z	Inertia momentum	$kg.m^2$
ν_t	Turbulent viscosity	$m^2.s^{-1}$
u_p	Piston speed	$m.s^{-1}$
C_μ	Turbulent viscosity constant	0,085
η	ε equation	$\eta = \sqrt{\frac{P_K}{m\nu_t}}\frac{k}{\varepsilon}$
η_0	ε equation	4,38
β	ε equation	0,012
$C_{\varepsilon 2}$	ε equation	1,68
$C_{\varepsilon 1}$	Production term P_ε	1,42
$C_{\varepsilon 4}$	Production term P_ε	-0,387
C_T	Tumble coefficient	Measured
C_{in}	In-cylinder energy loss	
C_a	MKE/TKE in-cylinder split coefficient	
C_b	Large to small scales time	
C_{len}	Length scale	
C_{tumb}	Tumble decay intensity	

m_e	Entrained gases mass	kg
m_b	Burned gases mass	kg
m_u	Fresh gases mass	kg
ρ_u	Fresh gases density	$kg.m^{-3}$
A_f	Unwrinkled flame area	m^2
S_L	Laminar flame speed	$m.s^{-1}$
S_T	Turbulent flame speed	$m.s^{-1}$
u'	Turbulence intensity	$m.s^{-1}$
r_f	Flame radius	m
l_t	Turbulent length scale	m
τ_{comb}	Characteristic combustion time	s
λ	Taylor microscale	m
μ_u	Viscosity	$kg.m^{-1}.s^{-1}$
C_s	Turbulent speed constant	$-$
C_k	Turbulent speed constant	$-$
C_λ	Characteristic combustion time constant	$-$

REFERENCES

[1] IEA, « CO2 Emissions from Fuel Combustion », 2018.

[2] PFA, « Contribution des véhicules légers et lourds à la réduction de la demande énergétique et des émissions de CO2 à horizon 2035 dans le monde », 2018.

[3] M. Vogler, A. Konigstein, et N. Fuhrmann, « Combustion Engines for Electrified Powertrains », *MTZ worldwide*, 2019.

[4] M. Ziegler, « Making Progress with Electrification », *MTZ worldwide*, 2019.

[5] M. Rode, T. Suzuki, G. Iosifidis, et T. Scheuermann, « Electric Turbocharger Concept for Highly Efficient Internal Combustion Engines », *MTZ Worldw*, vol. 80, n° 7, p. 120‑125, juill. 2019.

[6] D. Zi, L. Zhang, B. Chen, et Q. Zhang, « Study of the electric-booster and turbo-generator system and its influence on a 1.5 L gasoline engine », *Applied Thermal Engineering*, vol. 162, p. 114236, nov. 2019, doi: 10.1016/j.applthermaleng.2019.114236.

[7] R. Backhaus, « The Gasoline Engine Spark Ignition Remains », *MTZ worldwide*, 2019.

[8] V. Collée, C. Constensou, F. Dubois, et L. Guilly, « Variable Compression Ratio for Future Emission Standards », *MTZ Worldw*, vol. 78, n° 4, p. 52‑57, avr. 2017.

[9] S. Kiga, K. Moteki, et S. Kojima, « The New Nissan VC-Turbo with Variable Compression Ratio », *MTZ Worldw*, vol. 78, n° 11, p. 42‑49, nov. 2017.

[10] W. Schoeffmann *et al.*, « Dual Mode VCS – Vehicle Integration of a Modular VCR-System », présenté à SIA Powertrain and Electronics, Paris, 2019.

[11] C. Jung, A. Mudra, et D. Schulze, « Connecting rod for internal combustion engine with variable compression eccentrical element adjustment device », US10100725B2, oct. 16, 2018

[12] K. Wittek et F. Geiger, « Innovative Actuation Concepts for Variable-length Connecting Rods », *MTZ Worldw*, vol. 81, n° 12, p. 72‑77, déc. 2020, doi: 10.1007/s38313-020-0304-9.

[13] N. Morand, G. Agnew, N. Bontemps, et D. Jeckel, « Variable Nozzle Turbine Turbocharger for Gasoline" Miller" Engine », *MTZ worldwide*, vol. 78, n° 1, p. 40‑45, 2017.

[14] D. Dong, Y. Moriyoshi, et J. zhu, « To improve the performance of a variable geometry turbocharged SI Engine by porous material application », *Applied Thermal Engineering*, p. 117373, juill. 2021, doi: 10.1016/j.applthermaleng.2021.117373.

[15] W. Hannibal, R. Flierl, L. Stiegler, et R. Meyer, « Overview of Current Continuously Variable Valve Lift Systems for Four-Stroke Spark-Ignition Engines and the Criteria for their Design Ratings », SAE International, Warrendale, PA, SAE Technical Paper 2004-01‑1263, mars 2004.

[16] N. Zsiga, A. Omanovic, P. Soltic, et W. Schneider, « Functionality and Potential of a New Electrohydraulic Valve Train », *MTZ Worldw*, vol. 80, n° 9, p. 18‑27, sept. 2019.

[17] Q. Li, J. Liu, J. Fu, X. Zhou, et C. Liao, « Comparative study on the pumping losses between continuous variable valve lift (CVVL) engine and variable valve timing (VVT) engine », *Applied Thermal Engineering*, vol. 137, p. 710‑720, juin 2018, doi: 10.1016/j.applthermaleng.2018.04.017.

[18] Z. Lou et G. Zhu, « Review of Advancement in Variable Valve Actuation of Internal Combustion Engines », *Applied Sciences*, vol. 10, n° 4, Art. n° 4, janv. 2020, doi: 10.3390/app10041216.

[19] R. Koenen et J. Hansen, « Cylinder deactivation for a multiple cylinder engine », US20190107062A1, avr. 11, 2019 Consulté le: juill. 31, 2019. [En ligne]. Disponible sur: https://patents.google.com/patent/US20190107062A1/en

[20] T. Konrad, W. FIMML, et A. Bernhard, « Method for smoothly connecting a load during an activated cylinder deactivation process of an internal combustion engine », US20180128195A1, mai 10, 2018 Consulté le: juill. 31, 2019. [En ligne]. Disponible sur: https://patents.google.com/patent/US20180128195A1/en

[21] J. Zhao, Q. Xi, S. Wang, et S. Wang, « Improving the partial-load fuel economy of 4-cylinder SI engines by combining variable valve timing and cylinder-deactivation through double intake manifolds », *Applied Thermal Engineering*, vol. 141, p. 245‑256, août 2018, doi: 10.1016/j.applthermaleng.2018.05.087.

[22] K. Fridrichová, L. Drápal, J. Vopařil, et J. Dlugoš, « Overview of the potential and limitations of cylinder deactivation », *Renewable and Sustainable Energy Reviews*, vol. 146, p. 111196, août 2021, doi: 10.1016/j.rser.2021.111196.

[23] F. Hoppe, M. Thewes, H. Baumgarten, et J. Dohmen, « Water injection for gasoline engines: Potentials, challenges, and solutions », *International Journal of Engine Research*, vol. 17, n° 1, p. 86‑96, janv. 2016.

[24] S. Zhu *et al.*, « A review of water injection applied on the internal combustion engine », *Energy Conversion and Management*, vol. 184, p. 139‑158, mars 2019.

[25] Y. Zhuang *et al.*, « Investigation of water injection benefits on downsized boosted direct injection spark

ignition engine », *Fuel*, vol. 264, p. 116765, mars 2020, doi: 10.1016/j.fuel.2019.116765.
[26] R. Dauphin, D. Serrano, F. Guerbet, et L. Serve, « Fuel Formulations Based on RON Synergistic Effects for Better Fuel Economy and Lower CO2 Emissions », présenté à SIA Powertain and Electronics, Paris, 2019.
[27] M. Ziegler, « There is no alternative to this strategy », *MTZ Worldw*, vol. 80, n° 7, p. 54‑57, juill. 2019.
[28] W. Demmelbauer-Ebner, Jö. Theobald, Jö. Worm, et P. Scheller, « The new 1.5-l EA211 TGI evo », *MTZ Worldw*, vol. 79, n° 9, p. 16‑21, sept. 2018.
[29] I. T. Yilmaz, « The effect of hydrogen on the thermal efficiency and combustion process of the low compression ratio CI engine », *Applied Thermal Engineering*, vol. 197, p. 117381, oct. 2021, doi: 10.1016/j.applthermaleng.2021.117381.
[30] Q. Tang, P. Jiang, C. Peng, X. Duan, et Z. Zhao, « Impact of acetone–butanol–ethanol (ABE) and gasoline blends on the energy balance of a high-speed spark-ignition engine », *Applied Thermal Engineering*, vol. 184, p. 116267, févr. 2021, doi: 10.1016/j.applthermaleng.2020.116267.
[31] I. Hirose et M. Hitomi, « Mazdas way to more efficient ICE », *MTZ worldwide*, 2016.
[32] G. Bahng, D. Jang, Y. Kim, et M. Shin, « A new technology to overcome the limits of HCCI engine through fuel modification », *Applied Thermal Engineering*, vol. 98, p. 810‑815, avr. 2016, doi: 10.1016/j.applthermaleng.2015.12.076.
[33] M. Nishi, M. Kanehara, et N. Iida, « Assessment for innovative combustion on HCCI engine by controlling EGR ratio and engine speed », *Applied Thermal Engineering*, vol. 99, p. 42‑60, avr. 2016, doi: 10.1016/j.applthermaleng.2015.11.126.
[34] M. M. Hasan, M. M. Rahman, et M. G. Rasul, « The thermal and auto-ignition performance of a homogeneous charge compression ignition engine fuelled with diethyl ether and ethanol blends », *Applied Thermal Engineering*, vol. 190, p. 116828, mai 2021, doi: 10.1016/j.applthermaleng.2021.116828.
[35] « MWI Micro Wave Ignition AG – Mikrowellen-/ Raumzündungssysteme ». https://mwi-ag.com/
[36] J. Zembi, V. Cruccolini, F. Mariani, R. Scarcelli, et M. Battistoni, « Modeling of thermal and kinetic processes in non-equilibrium plasma ignition applied to a lean combustion engine », *Applied Thermal Engineering*, vol. 197, p. 117377, oct. 2021, doi: 10.1016/j.applthermaleng.2021.117377.
[37] S. Seyedkavoosi, S. Javan, et K. Kota, « Exergy-based optimization of an organic Rankine cycle (ORC) for waste heat recovery from an internal combustion engine (ICE) », *Applied Thermal Engineering*, vol. 126, p. 447‑457, nov. 2017, doi: 10.1016/j.applthermaleng.2017.07.124.
[38] J. Fu, J. Liu, Y. Yang, C. Ren, et G. Zhu, « A new approach for exhaust energy recovery of internal combustion engine: Steam turbocharging », *Applied Thermal Engineering*, vol. 52, n° 1, p. 150‑159, avr. 2013, doi: 10.1016/j.applthermaleng.2012.11.035.
[39] X. Ping *et al.*, « Prediction and optimization of power output of single screw expander in organic Rankine cycle (ORC) for diesel engine waste heat recovery », *Applied Thermal Engineering*, vol. 182, p. 116048, janv. 2021, doi: 10.1016/j.applthermaleng.2020.116048.
[40] W. Bou Nader, Y. Cheng, S. Houille, S. A. Belmedrek, et C. Dumand, « Methodology for the Optimization of the Overall Efficiency of a Combined Cycle: Internal Combustion Engine Coupled to Steam Rankine Cycle on Series Hybrid Electric Vehicles », présenté à SIA Powertrain and Electronics, Paris, 2019.
[41] E. Ortiz-Soto et M. Younkins, « Advanced Cylinder Deactivation with Miller Cycle », *MTZ worldwide*, 2019.
[42] N. Neumann, N. Freisinger, G. Vent, et T. Seeger, « Experimental investigation of Miller cycle combustion technology with water injection », in *19. Internationales Stuttgarter Symposium*, 2019, p. 599‑611.
[43] M. E. S. Martins et T. D. M. Lanzanova, « Full-load Miller cycle with ethanol and EGR: Potential benefits and challenges », *Applied Thermal Engineering*, vol. 90, p. 274‑285, nov. 2015.
[44] B. Wu, Q. Zhan, X. Yu, G. Lv, X. Nie, et S. Liu, « Effects of Miller cycle and variable geometry turbocharger on combustion and emissions in steady and transient cold process », *Applied Thermal Engineering*, vol. 118, p. 621‑629, mai 2017, doi: 10.1016/j.applthermaleng.2017.02.074.
[45] W. Ji, A. Li, X. Lu, Z. Huang, et L. Zhu, « Numerical study on NOx and ISFC co-optimization for a low-speed two-stroke engine via Miller cycle, EGR, intake air humidification, and injection strategy implementation », *Applied Thermal Engineering*, vol. 153, p. 398‑408, mai 2019, doi: 10.1016/j.applthermaleng.2019.03.035.
[46] K. Shen, Z. Xu, H. Chen, et Z. Zhang, « Investigation on the EGR effect to further improve fuel economy and emissions effect of Miller cycle turbocharged engine », *Energy*, vol. 215, p. 119116, janv. 2021, doi: 10.1016/j.energy.2020.119116.
[47] J. Atkinson, « Differential Engine », US336505A, févr. 16, 1886 Consulté le: févr. 05, 2019. [En ligne]. Disponible sur: https://patents.google.com/patent/US336505A/en
[48] J. Atkinson, « Cycle Engine », US367496A, août 02, 1887
[49] E. L. Marshall, « The Quest for Thermodynamic Efficiency: Atkinson Cycle Machines Versus Otto Cycle Machines », *The International Journal for the History of Engineering & Technology*, vol. 79, n° 1, p. 6‑33, janv. 2009.
[50] O. Dumbock, E. Schutting, H. Eichlseder, et W. Hubner, « Increasing the Efficiency of the Internal Combustion Engine through Extended Expansion », *MTZ worldwide*, 2018.
[51] « Honda Global | Exlink - Picture Book ». https://global.honda/innovation/technology/power/Exlink-picturebook.html
[52] S. Watanabe, H. Koga, et S. Kono, « Research on Extended Expansion General-Purpose Engine Theoretical Analysis of Multiple Linkage System and Improvement of Thermal Efficiency », *SAE Transactions*, vol. 115, p. 1124‑1131, 2006.
[53] « MCE5 VCRi », *MCE-5*. https://www.mce-5.com/vcri-taux-compression-variable-economie-carburant-reduction-co2-polluants/
[54] Y. Yamada, « Engine of compression-ratio variable type », US6820577B2, nov. 23, 2004 Consulté le: août 09, 2019. [En ligne]. Disponible sur: https://patents.google.com/patent/US6820577B2/en
[55] R. Miller, « High-pressure supercharging system », US2670595A, mars 02, 1954 Consulté le: août 09, 2019. [En ligne]. Disponible sur: https://patents.google.com/patent/US2670595A/en

[56] R. Miller, « High expansion, spark ignited, gas burning, internal combustion engines », US2773490A, déc. 11, 1956
[57] R. Miller, « Supercharged engine », US2817322A, déc. 24, 1957 Consulté le: août 09, 2019. [En ligne]. Disponible sur: https://patents.google.com/patent/US2817322A/en
[58] T. Johnen, « "Rightsizing" A Strategic Customer Interest », *MTZ Worldw*, vol. 77, n° 6, p. 90‑90, juin 2016.
[59] J. Sporleder, M. Alt, et T. Johnen, « The Efficient Gasoline Engines in the New Opel Astra K », *MTZ Worldw*, vol. 77, n° 2, p. 28‑33, févr. 2016.
[60] W. Demmelbauer-Ebner, K. Persigehl, M. Gorke, et E. Werstat, « The New 1.5-l Four-cylinder TSI Engine from Volkswagen », *MTZ Worldw*, vol. 78, n° 2, p. 16‑23, févr. 2017.
[61] R. Budack, R. Wurms, G. Mendl, et T. Heiduk, « The New Audi 2.0-l I4 TFSI Engine », *MTZ Worldw*, vol. 77, n° 5, p. 16‑23, mai 2016.
[62] S. Kallich, H. Graf, K. V. Schaller, et S. Ritter, « The New BMW Motorrad Boxer Engine with ShiftCam Technology », *MTZ worldwide*, vol. 80, n° 4, p. 32‑39, avr. 2019.
[63] M. Perceau, P. Guibert, et S. Guilain, « Modélisation 0D turbulente d'un moteur essence en vue de sa Millérisation », *Entropie : thermodynamique – énergie – environnement – économie*, vol. 1, n° 3, 2020, doi: 10.21494/ISTE.OP.2020.0577.
[64] H. P. Lenz, K. Wichart, et D. Gruden, « Variable Valve Timing—A Possibility to Control Engine Load without Throttle », *SAE Transactions*, vol. 97, p. 652‑658, 1988.
[65] R. Huber, P. Klumpp, et H. Ulbrich, « Dynamic Analysis of the Audi Valvelift System », *SAE International Journal of Engines*, vol. 3, n° 1, p. 839‑849, 2010.
[66] C. Brüstle et D. Schwarzenthal, « VarioCam Plus - A Highlight of the Porsche 911 Turbo Engine », SAE International, Warrendale, PA, SAE Technical Paper 2001-01‑0245, mars 2001.
[67] D. E. Foster, « An Overview of Zero-Dimensional Thermodynamic Models for IC Engine Data Analysis », *SAE Transactions*, vol. 94, p. 436‑449, 1985.
[68] F. Scappin, S. H. Stefansson, F. Haglind, A. Andreasen, et U. Larsen, « Validation of a zero-dimensional model for prediction of NOx and engine performance for electronically controlled marine two-stroke diesel engines », *Applied Thermal Engineering*, vol. 37, p. 344‑352, mai 2012, doi: 10.1016/j.applthermaleng.2011.11.047.
[69] I. W. S. L. Cruz, C. E. C. Alvarez, A. F. Teixeira, et R. M. Valle, « Zero-dimensional mathematical model of the torch ignited engine », *Applied Thermal Engineering*, vol. 103, p. 1237‑1250, juin 2016, doi: 10.1016/j.applthermaleng.2016.05.017.
[70] P. GUIBERT, « Modélisation du cycle moteur Approche zérodimensionnelle », *Techniques de l'ingénieur Combustion dans les moteurs thermiques et environnement*, vol. base documentaire : TIB166DUO., n° ref. article : bm2510, 2005.
[71] C. R. Ferguson et A. T. Kirkpatrick, *Internal Combustion Engines: Applied Thermosciences*. John Wiley & Sons, 2015.
[72] P. GUIBERT, « Modélisation du cycle moteur Moteurs à allumage commandé », *Techniques de l'ingénieur Combustion dans les moteurs thermiques et environnement*, vol. base documentaire : TIB166DUO., n° ref. article : bm2511, 2005.
[73] G. Woschni, « A Universally Applicable Equation for the Instantaneous Heat Transfer Coefficient in the Internal Combustion Engine », févr. 1967.
[74] S. G. Poulos et J. B. Heywood, « The Effect of Chamber Geometry on Spark-Ignition Engine Combustion », SAE International, Warrendale, PA, SAE Technical Paper 830334, févr. 1983.
[75] C. Borgnakke, V. S. Arpaci, et R. J. Tabaczynski, « A Model for the Instantaneous Heat Transfer and Turbulence in a Spark Ignition Engine », SAE International, Warrendale, PA, SAE Technical Paper 800287, févr. 1980.
[76] N. Fogla, M. Bybee, M. Mirzaeian, F. Millo, et S. Wahiduzzaman, « Development of a K-k-ϵ Phenomenological Model to Predict In-Cylinder Turbulence », *SAE International Journal of Engines*, vol. 10, n° 2, p. 562‑575, 2017.
[77] Y. Kim, M. Kim, S. Oh, W. Shin, S. Cho, et H. H. Song, « A New Physics-Based Modeling Approach for a 0D Turbulence Model to Reflect the Intake Port and Chamber Geometries and the Corresponding Flow Structures in High-Tumble Spark-Ignition Engines », *Energies*, vol. 12, n° 10, 2019.
[78] F. Bozza, L. Teodosio, V. D. Bellis, S. Fontanesi, et A. Iorio, « A Refined 0D Turbulence Model to Predict Tumble and Turbulence in SI Engines », *SAE Int. J. Engines*, vol. 12, n° 1, Art. n° 03-12-01‑0002, nov. 2018.
[79] « Flow Test Bench for Reserach & Development - AVL Tippelmann GmbH – Global leading manufacturer of High Quality Flow Test Benches ». https://www.avl-tippelmann.com/research-development.html
[80] Y. Kim, M. Kim, J. Kim, H. H. Song, Y. Park, et D. Han, « Predicting the Influences of Intake Port Geometry on the Tumble Generation and Turbulence Characteristics by Zero-Dimensional Spark Ignition Engine Model », 2018.
[81] F. Bozza, V. D. Bellis, F. Berni, A. D'Adamo, et L. Maresca, « Refinement of a 0D Turbulence Model to Predict Tumble and Turbulent Intensity in SI Engines. Part I: 3D Analyses », SAE International, Warrendale, PA, SAE Technical Paper 2018-01‑0850, avr. 2018.
[82] V. De Bellis, F. Bozza, S. Fontanesi, E. Severi, et F. Berni, « Development of a Phenomenological Turbulence Model through a Hierarchical 1D/3D Approach Applied to a VVA Turbocharged Engine », *SAE International Journal of Engines*, vol. 9, n° 1, p. 506‑519, 2016.
[83] R. J. Tabaczynski, C. R. Ferguson, et K. Radhakrishnan, « A Turbulent Entrainment Model for Spark-Ignition Engine Combustion », *SAE Transactions*, vol. 86, p. 2414‑2433, 1977.
[84] M. Mirzaeian, F. Millo, et L. Rolando, « Assessment of the Predictive Capabilities of a Combustion Model for a Modern Downsized Turbocharged SI Engine », avr. 2016.
[85] J. Heywood, *Internal Combustion Engine Fundamentals*. McGraw-Hill Education, 1988.
[86] F. M. White, *Fluid Mechanics*. McGraw Hill, 2011.